

ISSN 2095-1701

Volume 12 · Number 1 · March 2018



Engineering  
Transactions of CAE



11708

FRONTIERS IN ENERGY

Volume 12 ■ Number 1 ■ 2018 ■ pp 1-194

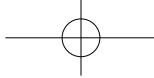
# Frontiers in Energy



Higher Education Press



Springer



# Frontiers in Energy

## Aims & Scope

*Frontiers in Energy*, a peer-reviewed international journal launched in January 2007, presents a unique platform for reporting the most advanced research and strategic thinking on energy technology. In its inaugural year it has published papers by internationally recognized authors in the field of energy development, particularly in China. It aims to promote rapid communication and dialogue among the researchers, scientists, engineers and policy makers working in the areas of energy and power engineering in China and abroad.

The Journal publishes review articles, original research papers and short communications by individual researchers and research groups. The journal is strictly peer-reviewed and accepts only original submissions in English.

The scope of the Journal covers fundamental energy science, energy technology (power generation, renewables, transport, urban design and building efficiency), environmental issues (pollution control, energy efficiency and climate change), and energy economics and policy. Interdisciplinary papers are encouraged.

## Supervised by

Ministry of Education of the People's Republic of China

## Sponsored by

Chinese Academy of Engineering

## Administered by

Higher Education Press, China  
Shanghai Jiao Tong University

## Submission information

Manuscripts should be submitted to  
<https://mc.manuscriptcentral.com/fie>

## Subscription information

**ISSN print edition: 2095-1701**

**ISSN electronic edition: 2095-1698**

## Subscription rates

For information on subscription rates please contact Springer Customer Service Center:  
[customerservice@springer.com](mailto:customerservice@springer.com)

## China

[customercenter@pub.hep.cn](mailto:customercenter@pub.hep.cn)

## Orders and inquiries

### 中国大陆地区

高等教育出版社

100029 北京市 朝阳区 惠新东街 4 号 富盛大厦 15 层

电话: +86-10-58556485

<http://journal.hep.com.cn>

The Americas (North, South, Central America and the Caribbean)

Springer Journal Fulfillment,

233 Spring Street, New York, NY, 10013-1578, USA

Tel. 800-SPRINGER (777-4643); 212-460-1500

(outside North America)

Outside the Americas

Springer Customer Service Center GmbH

Haberstr. 7, 69126 Heidelberg, Germany

Tel.: +49-6221-345-4303

## Journal website

[journal.hep.com.cn/fie](http://journal.hep.com.cn/fie)

[www.springer.com/journal/11708](http://www.springer.com/journal/11708)

## Electronic edition

An electronic version is available at

[journal.hep.com.cn/fie](http://journal.hep.com.cn/fie)

[link.springer.com/journal/11708](http://link.springer.com/journal/11708)

## Publication information

*Frontiers in Energy* is published 4 times a year.

Volume 12 (1–4 issues) will be published in 2018.

## Production

Higher Education Press

4 Huixin Dongjie, Beijing 100029, China

Printed in the People's Republic of China

## Jointly published by

Higher Education Press and Springer-Verlag GmbH Germany, part of Springer Nature

# Frontiers in Energy

---

## Editors-in-Chief

Shilie WENG Shanghai Jiao Tong University, China  
Weidou NI Tsinghua University, China  
Suping PENG China University of Mining and Technology (Beijing), China

## Executive Editor-in-Chief

Zhen HUANG Shanghai Jiao Tong University, China

## Deputy Editors-in-Chief

Yiguang JU Princeton University, USA  
Jing LIU Tsinghua University, China  
Yonglin JU Shanghai Jiao Tong University, China

## Members of Editorial Board

Radoslav ADZIC Brookhaven National Laboratory, USA  
Paul BRAUN University of Illinois at Urbana–Champaign, USA  
Xiaoshu CAI University of Shanghai for Science and Technology, China  
Kefa CEN Zhejiang University, China  
Qingquan CHEN The University of Hong Kong, China; China University of Mining and Technology (Beijing), China  
Yong CHEN Guangzhou Branch, Chinese Academy of Sciences, China  
Ping CHENG Shanghai Jiao Tong University, China  
Xu CHENG State Nuclear Power Research Institute, China  
Songyuan DAI North China Electric Power University, China  
Y Z DONG University of Sydney, Australia  
Weicheng FAN Tsinghua University, China  
Zhenping FENG Xi'an Jiaotong University, China  
Yong GENG Shanghai Jiao Tong University, China  
Minfang HAN Tsinghua University, China  
Yingduo HAN Tsinghua University, China  
Yassin A.HASSAN Texas A&M University, USA  
Yaling HE Xi'an Jiaotong University, China  
Qili HUANG State Grid Corporation of China, China  
Xiuchen JIANG Shanghai Jiao Tong University, China  
Xiumin JIANG Shanghai Jiao Tong University, China  
Yi JIANG Tsinghua University, China  
Hongguang JIN Institute of Engineering Thermophysics, Chinese Academy of Sciences, China  
Rafael KANDIYOTI Imperial College London, UK  
Chung K. LAW Princeton University, USA  
Gensheng LI China University of Petroleum (Beijing), China  
Jiangang LI Institute of Plasma Physics, Chinese Academy of Sciences, China  
Xianguo LI University of Waterloo, Canada  
Zheng LI Tsinghua University, China  
Zhengqi LI Harbin Institute of Technology, China  
Boqiang LIN Xiamen University, China  
Zonghu LIN University of Shanghai for Science and Technology, China  
Noam LIOR University of Pennsylvania, USA  
Hongtan LIU University of Miami, USA  
Zhongyang LUO Zhejiang University, China  
Toshio NAGASHIMA University of Tokyo, Japan  
Xianjue PENG China Academy of Engineering Physics, China  
Stratos PISTIKOPOULOS Imperial College London, UK  
Harald SCHWARZ Brandenburg University of Technology, Germany  
Wenzhong SHEN Shanghai Jiao Tong University, China  
Hongzhi SHENG Institute of Mechanics, Chinese Academy of Sciences, China  
Jinyuan SHI Shanghai Power Equipment Research Institute, China

Nickolay N. SMIRNOV	Moscow M.V. Lomonosov State University, Russia
Ulrich STIMMING	Newcastle University, UK
Wanhua SU	Tianjin University, China
Wenquan TAO	Xi'an Jiaotong University, China
Chengshan WANG	Tianjin University, China
Hai WANG	Stanford University, USA
Michael Quanlu WANG	Argonne National Laboratory, USA
Ruzhu WANG	Shanghai Jiao Tong University, China
Xueyou WEN	703 Institute, China Shipbuilding Industry Corporation, China
Kechang XIE	Taiyuan University of Technology, China; Chinese Academy of Engineering, China
Minghou XU	Huazhong University of Science and Technology, China
Xianfan XU	Purdue University, USA
Yusheng XUE	State Grid Electric Power Research Institute, China
Jinyue YAN	Mälardalen University, Sweden; Royal Institute of Technology, Sweden
Liangzhong YAO	China Electric Power Research Institute, China
Hong YANG	University of Illinois at Urbana–Champaign, USA
Baolian YI	Dalian Institute of Chemical Physics, Chinese Academy of Sciences, China
Naoto YORINO	Hiroshima University, Japan
Yixin YU	Tianjin University, China
Shiyi YUAN	China National Petroleum Corporation, China
Guangxi YUE	Tsinghua University, China
Hengyi ZENG	China National Offshore Oil Corporation, China
Junliang ZHANG	Shanghai Jiao Tong University, China
Yuzhuo ZHANG	The Shenhua Group Corporation Ltd., China
Zhuomin ZHANG	Georgia Institute of Technology, USA
Changying ZHAO	Shanghai Jiao Tong University, China
Tianshou ZHAO	Hong Kong University of Science & Technology, China
Dadi ZHOU	Energy Research Institute, National Development and Reform Commission, China
Shouwei ZHOU	State Key Laboratory of Oil and Gas Reservoir Geology and Exploitation, China
Yuan ZHOU	Technical Institute of Physics and Chemistry, Chinese Academy of Sciences, China

#### **Managing Editors**

Xiaoyan QIAO	Higher Education Press, China
Dongping HUANG	Shanghai Jiao Tong University, China
Shaoyun YAN	Shanghai Jiao Tong University, China
Ruiqin LIU	Shanghai Jiao Tong University, China
Xiaoqing LI	Shanghai Jiao Tong University, China

---

# Copyright Information

## For Authors

As soon as an article is accepted for publication, authors will be requested to assign copyright of the article (or to grant exclusive publication and dissemination rights) to the publisher (respective the owner if other than Springer). This will ensure the widest possible protection and dissemination of information under copyright laws.

More information about copyright regulations for this journal is available at [www.springer.com/journal/11708](http://www.springer.com/journal/11708).

## For Readers

While the advice and information in this journal is believed to be true and accurate at the date of its publication, neither the authors, the editors, nor the publisher can accept any legal responsibility for any errors or omissions that may have been made. The publisher makes no warranty, express or implied, with respect to the material contained herein.

All articles published in this journal are protected by copyright, which covers the exclusive rights to reproduce and distribute the article (e.g., as offprints), as well as all translation rights. No material published in this journal may be reproduced photographically or stored on microfilm, in electronic data bases, on video disks, etc., without first obtaining written permission from the publisher (respective the copyright owner if other than Springer). The use of general descriptive names, trade names, trademarks, etc., in this publication, even if not specifically identified, does not imply that these names are not protected by the relevant laws and regulations.

Springer has partnered with Copyright Clearance Center's RightsLink service to offer a variety of options

for reusing Springer content. For permission to reuse our content please locate the material that you wish to use on [link.springer.com](http://link.springer.com) or on [springerimages.com](http://springerimages.com) and click on the permissions link or go to [copyright.com](http://copyright.com) and enter the title of the publication that you wish to use. For assistance in placing a permission request, Copyright Clearance Center can be contacted directly via phone: +1-855-239-3415, fax: +1-978-646-8600, or e-mail: [info@copyright.com](mailto:info@copyright.com).

## Copyright Holder and Copyright Year

Higher Education Press and Springer-Verlag GmbH Germany, part of Springer Nature 2018

## Disclaimer

Springer publishes advertisements in this journal in reliance upon the responsibility of the advertiser to comply with all legal requirements relating to the marketing and sale of products or services advertised. Springer and the editors are not responsible for claims made in the advertisements published in the journal. The appearance of advertisements in Springer publications does not constitute endorsement, implied or intended, of the product advertised or the claims made for it by the advertiser.

## Office of Publication

Springer-Verlag GmbH, Tiergartenstraße 17, 69121 Heidelberg, Germany

Higher Education Press

4 Huixin Dongjie, Beijing 100029, China

Printed in the People's Republic of China

Yangsuo XIE\*, Bowen ZHU\*, Jing LIU, Zaoli XU, Xinwei WANG

# Thermal reffusivity: uncovering phonon behavior, structural defects, and domain size

© Higher Education Press and Springer-Verlag GmbH Germany, part of Springer Nature 2018

**Abstract** To understand the relation between different nanostructures and thermal properties, a simple yet effective model is in demand for characterizing the underlying phonons and electrons scattering mechanisms. Herein, we make a systematic review on the newly developed thermal reffusivity theory. Like electrical resistivity which has been historically used as a theory for analyzing structural domain size and defect levels of metals, the thermal reffusivity can also uncover phonon behavior, structure defects and domain size of materials. We highlight that this new theory can be used for not only metals, but also nonmetals, even for amorphous materials. From the thermal reffusivity against temperature curves, the Debye temperature of the material and the ideal thermal diffusivity of single perfect crystal can be evaluated. From the residual thermal reffusivity at the 0 K limit, the structural thermal domain (STD) size of crystalline and amorphous materials can be obtained. The difference of white hair and normal black hair from heat conduction perspective is reported for the first time. Loss of melanin results in a worse thermal protection and a larger STD size in the white hair. By reviewing the different variation of thermal reffusivity against decreasing temperature profiles, we conclude that they reflected the structural connection in the materials. Ultimately, the future application of thermal reffusivity theory in studying 2D materials and amorphous materials is discussed.

**Keywords** thermal reffusivity theory, phonon behavior,

Received Jul. 5, 2017; accepted Sep. 20, 2017; online Jan. 5, 2018

Yangsuo XIE  
College of Chemistry and Environmental Engineering, Shenzhen University, Shenzhen 518055, China

Bowen ZHU, Jing LIU, Zaoli XU, Xinwei WANG (✉)  
Department of Mechanical Engineering, 2025 Black Engineering Building, Iowa State University, Ames, IA 50011, USA  
E-mail: xwang3@iastate.edu

\*These authors contributed equally to this work.

structure defects, structural thermal domain (STD) size, 2D material, amorphous material

## 1 Introduction

In recent years, promoted by the increasing demands of applications in different fields, such as in electronics thermal dissipation, thermal protection, as well as thermo-electric sensing, different innovative materials have been synthesized and extensively studied. The thermal property among other important properties of these materials becomes increasingly important for their applications. Thermal conductivity ( $\kappa$ ) and diffusivity ( $\alpha$ ) of solids depend on their inner structures, which includes the structural domain size, defects densities, and strength of interconnection among nanoparts, etc. Despite the reported complex phonon/electron modeling, to have a better understanding of the relation between different structures and heat conduction, a simple yet effective model is required. Phonons and electrons are the two main types of heat carriers contributing to  $\kappa$  of different materials. During propagation, phonons and electrons diffuse through materials, suffering from frequent collisions. The scattering can be divided into two categories: scattering by phonons (Umklapp scattering) and defect scattering (by lattice defects, chemical impurities, grain boundaries, and rough edges, etc.). From kinetic theory of gases, the resulting thermal conductivity can be expressed as  $\kappa = Cv l_s/3$ , where  $C$  is the energy carriers' heat capacity per unit volume,  $v$  is the average particle velocity, and  $l_s$  is the mean free path of the particles between two consecutive collisions.

For most nonmetallic crystals, phonons are the main heat carriers. A phonon is a quantum mechanical description of lattice vibrational motion in which a lattice of atoms/moleculars oscillates at a single frequency [1]. Phonons are often designated as quasiparticles and obey Bose-Einstein distribution. They play an important role as energy carrier in heat capacity and thermal conductivity in

condensed phase. For phonons, the collisions are sourced from not only other phonons, but also from lattice defects, chemical impurities, grain boundaries, and rough edges, etc. In the past, researchers had a glimpse of phonon scattering mechanisms from  $\kappa$ - $T$  profiles [2,3]. At low temperatures, the defect scattering becomes dominant and the  $l_s$  value is expected to be constant. As a result, the  $\kappa$ - $T$  profiles at low temperatures are expected to vary as  $C$ - $T$  profiles. However, due to the complexity of  $C$ - $T$  profiles, the phonon scattering mechanisms cannot be directly evaluated. Sometimes, the mean free path  $l_s$  is used for studying the phonon scattering. It directly reflects the average distance between two consecutive collisions and can be used as a measure of structural domain size. However, it is hard to measure and so the application is limited. Besides  $\kappa$ , another important physical term  $\alpha$  is defined as  $\kappa$  divided by the density and specific heat capacity at constant pressure:  $\alpha = \kappa/\rho c_p$ . Considering the relation of  $\kappa = C v l_s/3$ ,  $\alpha$  is a function of  $v$  and  $l_s$ :  $\alpha = v l_s/3$ . However, this relation has been rarely used.

In pure metals, electrons are the main heat carriers. While in impure metals or disordered alloys, contribution from phonons may be comparable with that from electrons [4]. The  $\kappa$ - $T$  profile of metals gives very little information about the electrons scattering. In metals, electrons make a dominant contribution to the  $\kappa$ . From  $\kappa = C v l_s/3$ , we have  $\kappa = C_e v_F^2 \tau/3$ . In this equation,  $C_e$  is the electron volumetric heat capacity,  $v_F$  is the Fermi velocity, and  $\tau$  is the electron relaxation time [5]. Thus, the  $\kappa$ - $T$  curve is not only determined by the electron scattering time, but also hinges on the evolution of  $C_e$ , which is also a function of temperature. Between the Debye temperature and the Fermi temperature, the bulk heat capacity of metals ( $C_v$ ) is a sum of electron and phonon contribution:  $C_v = \gamma T + AT^3$ , in which the first term is from electrons and the latter one is from phonons [5]. At relatively high temperatures, the phonon contribution is more significant than that of electron. Thus,  $\alpha$ - $T$  curve reflects a combined effect of electron scattering and phonon heat capacity. The thermal diffusivity ( $\alpha$ ) of metals cannot be used to characterize the electron scattering either.

Electron scattering mechanisms and intensities have historically been studied and used for analyzing structures in metals. The total electrical resistivity ( $\rho_e$ ) comes from mechanisms assumed to contribute to electron scattering: an isotropic contribution from phonons scattering; a contribution due to grain boundaries; a contribution from external surfaces [6], and from chemical impurities and lattice defects. The  $\rho_e$ - $T$  profiles provide unprecedented details of the electron scattering. The temperature dependent part at high temperatures is dominated by electron-phonon scattering and is proportional to the phonon concentration. Also the slope of  $\rho_e$ - $T$  can be used for extracting the Debye temperature. In addition, the residual resistivity value at the 0 K limit reflects defects

and impurities scattering intensity. The resistivity ratio which is defined as the ratio of the total resistivity at RT to the residual resistivity at 0 K has been a convenient indicator of materials' purity. Thus, the experimental  $\rho_e$ - $T$  curves and the corresponding theoretical model provide a good way for studying the electron scattering mechanisms and structure of metals. However, for electrically non-conductive materials, the  $\rho_e$ - $T$  data becomes less straightforward and useful. Furthermore, since the electrical transport model of semiconductors is different from metals, the  $\rho_e$ - $T$  curve does not follow the physical model of metals either. Therefore, for nonmetals, this method becomes less applicable. The  $\rho_e$ - $T$  curves and the corresponding theoretical model of metals will be introduced in detail in Section 2.

In summary, there have not been many simple physical terms or models to directly and conveniently characterize the phonon/electron scattering mechanisms, structural defects, and domain sizes of different materials. Although for pure metals, the  $\rho_e$ - $T$  curves provide an excellent way for evaluating the purity and electron scattering, it is not applicable for semi-conductors or nonconductors. The understanding of the phonons/electrons scattering plays an essential role in analyzing and predicting the thermal behaviors of different materials. Thus, it is in demand to develop a model to answer all the requirements. Therefore, a new thermal reffusivity theory has been developed in recent years and it provided an effective method for characterizing the phonons/electrons scattering, structural defects, and domain sizes of different kinds of materials.

In this work, we first review the relation between electrical resistivity and structures. Then we introduce the principle of thermal reffusivity by examining the studies on the structural defect levels using thermal reffusivity model. The studied materials include silver/silver nanowire, graphene foam, partly reduced graphene paper/graphene oxide paper/graphene paper, polyethylene materials, and pre/post-annealed carbon fibers, etc. In addition, the application of thermal reffusivity for evaluating the Debye temperature of materials, and estimating the ideal thermal diffusivity of materials with perfect single crystal is reviewed. More importantly, we highlight the application of the residual thermal reffusivity in characterizing the structural thermal domain (STD) size in not only crystalline materials but also amorphous materials. We explore the physical meaning and validation of the STD size by comparing with the crystallite size reported from XRD result. To provide an example for the application of thermal reffusivity in characterizing the domain size of amorphous materials, we conduct a study on human hair of black and white color. The difference of white hair and normal black hair from heat conduction perspective is reported for the first time. Finally, we discuss the future applications of this theory in studying new 2D materials and amorphous

materials, as well as in providing experimental reference for calculation.

## 2 Electron transport and structure

Electrical resistivity has been historically utilized for analyzing structures in metals.  $\rho_e$  is an intrinsic property that quantifies the ability of a given material to opposes the flow of electrical current. It is defined as  $\rho_e = RA/L$ , in which  $R$  is the electrical resistance of a uniform specimen,  $L$  is the length and  $A$  is the cross-sectional area. For simple metals,  $\rho_e$  increases with temperature. At higher temperatures,  $\rho_e$  has a linear relationship with temperature. At low temperature,  $\rho_e$  follows a power law function of temperature whose shape can be characterized by the Bloch-Grüneisen formula:

$$\rho_e = \rho_0 + \alpha_p \left( \frac{T}{\theta_R} \right)^5 \int_0^{\theta_R/T} \frac{x^5}{(e^x - 1)(1 - e^{-x})} dx, \quad (1)$$

where  $\alpha_p$  is a constant and  $\theta_R$  is the Debye temperature.  $\alpha_p$  is proportional to the electron-phonon coupling constant  $\lambda_{tr}$  and Debye frequency  $\omega_D$ , and inversely proportional to the squared Drude plasma frequency  $\omega_p$  [7]. From the  $\rho_e$ - $T$  profiles of different metal specimens,  $\rho_e$  approaches a constant value  $\rho_0$  as temperature reduces to 0 K.  $\rho_0$  is entitled as “residual electrical resistivity.” It is caused by defect scattering (grain boundary scattering, lattice defects, chemical impurities scattering, and surface scattering) whose intensity is determined not only by the type of metal, but also by its purity and structural domain size. From Matthiessen’s rule, the total electrical resistivity of simple metals can be approximated as the sum of  $\rho_0$  and the intrinsic electrical resistivity  $\rho_i$  as  $\rho_e = \rho_i + \rho_0$ , where  $\rho_i$  originates from the scattering by phonons.

Since  $\rho_0$  is generally independent of temperature and determined by defect scattering, its value can be used to characterize the level of structural defects in metal specimens. The proportion of  $\rho_0$  over the total  $\rho_e$  at RT can be used as a quantitative measure of the structural defects in metal specimens. Xu et al. [8] measured the  $\rho_e$ - $T$  profile of Ir film on DNA fibers and compared with that of bulk Ir from RT down to 10 K. The result is shown in Fig. 1(a). In Xu’s work, the nanoscale Ir film on DNA fibers had a much higher  $\rho_0$  value than that of the bulk specimen. For Ir film,  $\rho_0$  was around  $22 \times 10^{-8}$ – $33 \times 10^{-8} \Omega \cdot m$ , while for bulk Ir,  $\rho_0$  was less than  $5 \times 10^{-9} \Omega \cdot m$ . The  $\rho_0/\rho_e$  ratio of Ir film was about 85.5% and 78.9% for fiber 1 and 2 respectively. For the bulk Ir, the  $\rho_0/\rho_e$  ratio was less than 5%. The over 15-fold higher  $\rho_0/\rho_e$  ratio illustrates that the intensity of defect scattering in the nanoscale Ir film is much higher than that in the bulk Ir. This result is reasonable since the Ir film was sputtered onto the DNA fibers, which inevitably contained lattice defects and impurities. Meanwhile, due to the size effect, the nanoscale

film has a much higher surface/volume ratio, which leads to a higher level of grain boundary scattering in nanoscale Ir film.

Combined with the Bloch-Grüneisen formula fitting, the Debye temperature  $\theta_R$  and  $\alpha_p$  can also be evaluated. The solid lines in Fig. 1(a) are the Bloch-Grüneisen formula fitting using Eq. (1). The resulting  $\rho_e$ - $T$  curves of nanoscale Ir film and bulk Ir were parallel. For the two bulk Ir specimen, the fitting gave the  $\alpha_p$  value of  $21.86 \times 10^{-8}$ – $22.34 \times 10^{-8} \Omega \cdot m$ , and  $\theta_R$  value of 306.1–307.6 K. For nanoscale Ir film on DNA fibers, the fitting result was  $21.96 \times 10^{-8}$ – $22.49 \times 10^{-8} \Omega \cdot m$  for  $\alpha_p$ , and 259.4–285.9 K for  $\theta_R$ . Xu’s value was close to the value measured from specific heat of high-temperature range (290 K) [8,9]. Thus, the  $\rho_e$ - $T$  model provided an alternative way for evaluating  $\theta_R$ .

The parallel  $\rho_e$ - $T$  profiles are expected only if the two specimens share the same  $\theta_R$  and  $\alpha_p$ . Even for the same type of simple metal specimens, most of the  $\rho_e$ - $T$  could be nonparallel. The Debye temperature reflects the connection strength of grains in the specimens. When the connection weakens (the phonon softening), the Debye temperature decreases. In addition, Xu et al. tested the  $\rho_e$ - $T$  profiles of Ir nanofilm on different substrate fibers, including glass fiber, milk weed, and spider silk. The resulting slope of  $\rho_e$ - $T$  is one-fold lower than that of the bulk Ir. This was due to the quantum confinement of nanoscale materials, which changes the distribution of phonon frequency with wavelength. Under this circumstance, the phonon-electron scattering mechanisms will be different, which leads to nonparallel  $\rho_e$ - $T$  curves. DNA provides extra channels for electron transport by thermal hopping and quantum tunneling, which could largely weaken the quantum effect. Cheng et al. [10] reported the  $\rho_e$ - $T$  curve of single polycrystalline silver nanowire from RT to 35 K. The result is shown in Fig. 1(b). The slope of  $\rho_e$  against  $T$  of the silver nanowire ( $1.68 \times 10^{-10} \Omega \cdot m/K$ ) was much larger than that of the bulk silver ( $6.11 \times 10^{-11} \Omega \cdot m/K$ ). The larger slope was attributed to the enhanced electron-phonon coupling and the surface phonon softening in silver nanowire. Even though nonparallel, the proportion of  $\rho_0$  over the total  $\rho_e$  at RT can still be used as a measure of structural defect levels. In Cheng’s work,  $\rho_0$  of the bulk silver was almost zero, while  $\rho_0$  of the silver nanowire was much higher ( $3.25 \times 10^{-8} \Omega \cdot m$ ), which takes about 42.2% over the total  $\rho_e$  at RT. This shows a much higher level of structural defect in silver nanowire than bulk silver.

$\rho_e$  of metals can be expressed in terms of the mean scattering time of electrons ( $\tau$ ) as  $\rho_e = m/ne^2\tau$ , in which  $m$  and  $e$  are the electron mass and charge respectively, and  $n$  is the electron density. Thus,  $\rho_0$  can also be expressed as a function of  $\tau_0$  as  $\rho_0 = \frac{m}{ne^2}\tau_0^{-1}$ . Here  $\tau_0$  is the mean scattering time induced solely by defect scattering. Combined with the Fermi velocity  $v$ , the electron mean free path induced solely by the defect scattering can be

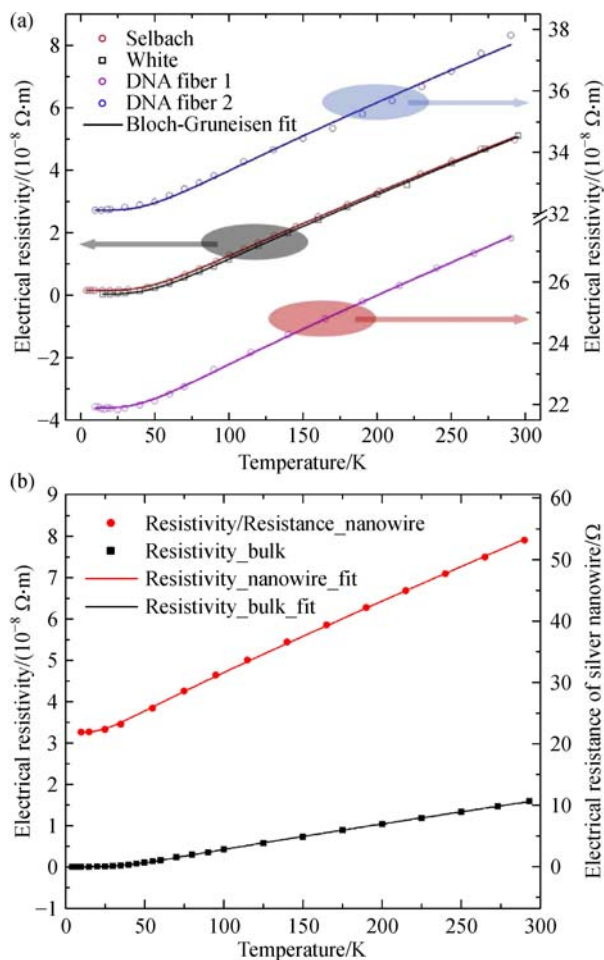


**Fig. 1** The  $\rho_e$ - $T$  profile of nanoscale metal and compared with that of bulk metal from RT down to 10 K

(a) Temperature dependent electrical resistivity of bulk Ir and nanoscale Ir film on DNA fibers [8]. (Reprinted from Polymer, 55, Xu et al., Promoted electron transport and sustained phonon transport by DNA down to 10 K, 6373-6380, Copyright (2014), with permission from Elsevier.); (b) “Temperature dependent electrical resistivity of the silver nanowire and bulk silver” by Cheng et al. [10] is licensed under CC BY. Solid curves are the Bloch-Grüneisen formula fitting.

evaluated, which reflects an effective structural domain size. In Cheng’s work, they calculated the electron mean free path of silver nanowire based on the experimentally measured  $\rho_0$  value. The resulting value was 26 nm, which was close to the crystal size evaluated from XRD results (21 nm) [10]. Therefore, the experimental data of  $\rho_e$ - $T$  profiles can be used to effectively characterize the structural defect levels, the Debye temperature, and the structural domain size in simple metals.

### 3 Thermal reffusivity: electrons

From the above analysis,  $\rho_e$  is very effective in evaluating the defect level, the Debye temperature, and the structural

domain size of metals. However, for electrically non-conductive materials or semiconductors, this method becomes not applicable. Although electrically nonconductive, the thermal conductivity and diffusivity of these materials are readily measurable. Based on the understanding of electron/phonon scattering, a new physical term called ‘thermal reffusivity’ from heat conduction perspective has been proposed and developed to characterize the defect level, the Debye temperature, and the structural domain size of various materials.

As illustrated in the introduction, if we directly look at the  $\kappa$ - $T$  or  $\alpha$ - $T$  profile of metals, very little information about the electron scattering mechanisms and intensities can be obtained. The  $\kappa$ - $T$  curve is not only determined by the relaxation time of electrons, but also hinges on the  $C_e$  evolution. To study the electron scattering time directly, the effect of  $C_e$  needs to be taken out.  $C_e$  is a function of temperature as  $C_e = \gamma T$ , in which  $\gamma$  is a constant. Under this circumstance, a new physical term called ‘unified thermal resistivity’ for metals was first defined by Cheng et al. [10] as

$$\Theta = T/\kappa. \quad (2)$$

Combining with equation  $\kappa = C_e v_F^2 \tau / 3$ ,  $\Theta$  becomes a function of  $\tau$  as

$$\Theta = \frac{3}{\gamma v_F^2} \tau^{-1}. \quad (3)$$

By studying the  $\Theta$ - $T$  curve, the different electron scattering mechanisms and corresponding intensities can be elucidated [10]. The physical meaning of  $\Theta$  can be interpreted as the thermal resistance per unit specific heat of electrons. Note this “unified thermal resistivity” shares the same meaning of the “thermal reffusivity” introduced for phonons.

Cheng et al. measured the  $\kappa$ - $T$  and  $\Theta$ - $T$  curve of silver nanowire and compared with that of bulk silver. The result is presented in Fig. 2 [10]. The  $\kappa$ - $T$  curves of the silver nanowire and bulk silver did not have a lot in common as is shown in Fig. 2(a). The  $\kappa$  of silver nanowire was much lower than that of bulk silver. The  $\kappa$  of bulk silver increased as temperature goes down, while the  $\kappa$  of silver nanowire presented a reversed behavior. From the  $\kappa$ - $T$  curves, the information about the structures and electron scattering mechanism are very limited. For comparison, Fig. 2(b) showed the  $\Theta$ - $T$  curve. The  $\Theta$ - $T$  curves of both materials showed a similar linearly decreasing pattern as temperature goes down to about 60 K. The slope of  $\Theta$ - $T$  is  $2.57 \times 10^{-3} \text{ m} \cdot \text{K}/\text{W}$  for silver nanowires and  $2.41 \times 10^{-3} \text{ m} \cdot \text{K}/\text{W}$  for bulk silver, which were almost the same. The only difference was in the magnitude of  $\Theta$ . Thus, the  $\Theta$ - $T$  curves showed much more similarities for the same type of metals.

Same as that for  $\rho_e$ , the Mathiessen’s rule can be applied to separate the effect of electron-phonon scattering and

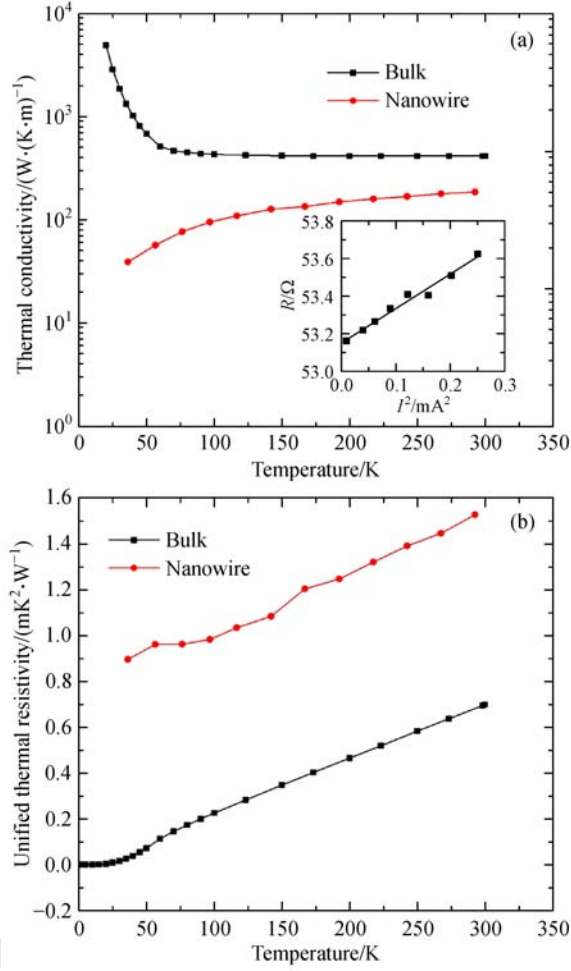


**Fig. 2** The  $\kappa$ - $T$  and  $\Theta$ - $T$  curve of silver nanowire and compared with that of bulk silver

(a) Temperature dependent thermal conductivity of the silver nanowire and bulk silver; (b) Temperature dependent unified thermal resistivity of the silver nanowire and bulk silver (by Cheng et al. is licensed under CC BY [10])

defect scattering. Therefore,  $\Theta$  can be written as

$$\Theta = \frac{3}{\gamma V_F^2} (\tau_{\text{phonon}}^{-1} + \tau_{\text{defect}}^{-1}). \quad (4)$$

Here  $\tau_{\text{phonon}}^{-1}$  is from electron-phonon scattering, and  $\tau_{\text{defect}}^{-1}$  is from defect scattering. At higher temperatures,  $\tau_{\text{phonon}}^{-1}$  dominates. As temperature approaches 0 K,  $\tau_{\text{phonon}}^{-1}$  vanishes and  $\tau_{\text{defect}}^{-1}$  dominates. Therefore, a residual value ( $\Theta_0$ ) which corresponds to the defect scattering intensity can be measured at low temperatures. Just like the residual electrical resistivity, this  $\Theta_0$  also reflects the defect scattering influence as

$$\Theta_0 = \frac{3}{\gamma V_F^2} \tau_{\text{defect}}^{-1}. \quad (5)$$

The parallel  $\Theta$ - $T$  curves in Cheng et al.'s work

(Fig. 2(b)) illustrates that the silver nanowires and bulk silver shared the similar phonon-electron scattering mechanism. The intensity of defect scattering kept constant as temperature changes. On the other hand, the slope of the  $\rho_e$ - $T$  curves of silver nanowire and bulk silver (Fig. 1(b)) is quite different. This is a very interesting phenomenon which indicated that the electron scattering contributed to electrical and thermal transport differently. Cheng et al. [10] ascribed this difference to the change of electron-phonon coupling strength induced by the structural disorder and quantum size effect in nanoscale silver. As illustrated before, the  $\rho_e$ - $T$  curves would be parallel only if the two materials shared the same  $\theta_R$  and  $\alpha_p$  value. The slope of the  $\Theta$ - $T$  curves reflects more complex electron-phonon interaction. A more comprehensive understanding requires further future work.

$\Theta_0$  value reflects the defect scattering influence. For the same kind of metal, the proportion of  $\Theta_0$  is a quantitative measure of the defect levels in the materials. From Cheng et al.'s work,  $\Theta_0$  value of the silver nanowire and the bulk silver were quite different. As temperature reduced,  $\Theta$  of bulk silver goes to zero, while  $\Theta$  of the silver nanowire approaches about 0.9 m·K<sup>2</sup>/W at 30 K for the silver nanowire. This showed that the defect scattering intensity in the silver nanowire was much higher than that in bulk silver specimen. The grain boundary effect was significant in nanoscale materials which leads to much higher defect scattering than that in the bulk materials. In addition, there were more lattice defects and impurities in the nanoscale materials which provided more scattering sites. From these results, the defect level in the silver nanowire is much higher than that in bulk silver. This conclusion is consistent as that from the  $\rho_e$ - $T$  study. Thus, the thermal reffusivity theory offers an alternative and effective way for the  $\rho_e$ - $T$  theory for metals.

## 4 Thermal reffusivity: phonons

For semiconductors and nonconductors, phonons are the main heat carriers. For a crystal with at least two atoms in primitive cell, there are two types of phonons: optical phonons and acoustic phonons. The phonon propagation is not only limited by other phonons scattering, but also by defect scattering including chemical impurities, grain boundaries, lattice defects, and rough edges. Collisions of phonons which conserve the phonon momentum is called normal scattering (N-scattering), while that change the total phonon momentum is called Umklapp scattering (U-scattering). Generally, N-scattering is ignored in favor of the U-scattering. To participate in the U-process, the energy of phonons needs to be in the order of  $\frac{1}{2}k_B\theta$ , in which  $k_B$  is Boltzmann's constant, and  $\theta$  is the Debye temperature [5]. At high temperatures, all phonons are excited. Therefore, the U-scattering dominates the thermal

transport at high temperatures. At low temperatures, the phonon population participating in U-scattering can be roughly estimated as  $\sim e^{\theta/2T}$  according to the Boltzmann factor [11]. At low temperatures, due to the largely reduced phonon population in U-scattering, the U-scattering becomes ineffective in limiting the phonon propagation. Under this circumstance, the defect scattering becomes dominant.

To characterize the phonon scattering intensities, ‘thermal reffusivity’ of phonons was defined first by Xu et al. [8] as

$$\Theta = 1/\alpha. \quad (6)$$

Here  $\alpha$  is thermal diffusivity. From Mathiessen rule, the influence of different scattering mechanisms can be linearly added for the total scattering effect. If we express this in terms of the scattering time, then:

$$\frac{1}{\tau} = \frac{1}{\tau_{\text{phonon}}} + \frac{1}{\tau_{\text{impurities}}} + \frac{1}{\tau_{\text{grain}}} + \frac{1}{\tau_{\text{defect}}} + \frac{1}{\tau_{\text{surfaces}}} + \dots \quad (7)$$

Thus, combining Eqs. (6) and (7), thermal reffusivity of phonons can be written as

$$\Theta = \frac{3}{v^2} \left( \frac{1}{\tau_{\text{phonon}}} + \frac{1}{\tau_{\text{impurities}}} + \frac{1}{\tau_{\text{grain}}} + \frac{1}{\tau_{\text{defect}}} + \frac{1}{\tau_{\text{surfaces}}} + \dots \right). \quad (8)$$

Since the phonon population in U-scattering follows a behavior of  $e^{-\theta/2T}$  (sometimes  $e^{-\theta/3T}$ ), when temperature is much lower than  $\theta$ ,  $\tau_{\text{phonon}}^{-1}$  value is also expected to present a temperature dependence as  $\sim e^{-\theta/2T}$ . By contrast, the relaxation time from structural defects are almost independent on temperature. If the phonon velocity  $v$  of a material is independent of temperature (which is a good approximation for most of materials),  $\Theta$  of phonons can be expressed as a function of temperature as

$$\Theta = \Theta_0 + C \times e^{-\theta/2T}. \quad (9)$$

This equation is the thermal reffusivity model of phonons. As indicated in this equation, the overall thermal reffusivity of a material will decrease as temperature goes down and finally reaches a constant value ( $\Theta_0$ ) at the 0 K limit.  $\Theta_0$  is entitled as residual thermal reffusivity. Just like  $\Theta_0$  of electrons, this  $\Theta_0$  reflects only defect scattering influence. The proportion of  $\Theta_0$  over the total  $\Theta$  at RT can also be used as a quantitative measure of the defect levels in nonmetallic crystals. Therefore, this thermal reffusivity model significantly broadens the scope of application of  $\rho_c$  model introduced in Section 2.

The  $\Theta$ - $T$  profiles of different materials whose thermal transport is dominated by phonons have been measured

experimentally. By fitting the experimental data with the thermal reffusivity model expressed in Eq. (9), the  $\Theta_0$  value, the defect levels, and  $\theta$  were extracted. Take an extreme example, for some crystalline materials with negligible defects, such as silicon, germanium, sodium chloride, and sodium fluoride crystals, the  $\Theta_0$  value was measured to be almost zero. For other materials with some levels of defects, the resulting  $\Theta_0$  values were reported to be finite constants. Xie et al. [12] measured the  $\Theta$ - $T$  curves of graphene foam (GF) material grown by the chemical vapor deposition method, and calculated the  $\Theta$ - $T$  curves of three different pyrolytic graphite materials according to the experimental data published in literatures. The results are summarized in Fig. 3. The fitting lines by the thermal reffusivity model are also presented in the figures, which gave excellent fittings for all the experimental data. From the fitting result of GF:  $\Theta = 1878 + 1.03 \times 10^5 \times e^{-906.6 \times T}$ , the  $\Theta_0$  value was 1878 s/m, which took 27.2% of the total  $\Theta$  at RT ( $\Theta_{\text{RT}}$ ). For comparison, the data of pyrolytic graphite materials from Ho et al., Hooker et al., and Slack et al. gave a  $\Theta_0$  value of 43.3–112.1 s/m, which took only 5%–14% of  $\Theta_{\text{RT}}$ . The  $\Theta_0/\Theta_{\text{RT}}$  ratio of GF was 2–5 times higher than that of pyrolytic graphite. Therefore, the defect levels in GF was quantitatively measured to be 2–5 times higher than that in the three pyrolytic graphite materials [12].

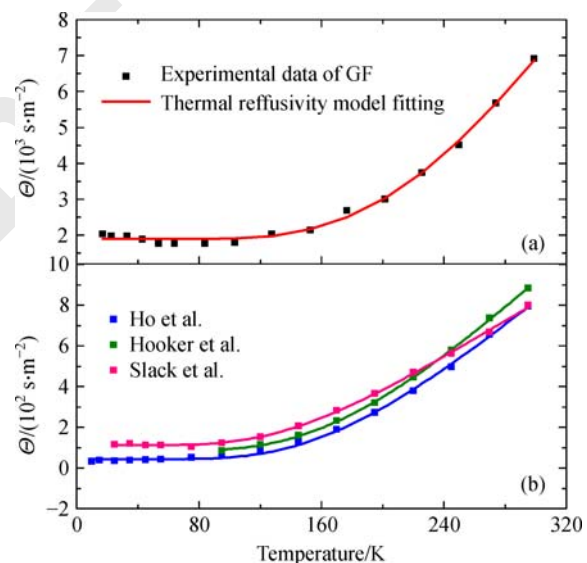


**Fig. 3** Thermal reffusivity against temperature profile (a) Graphene foam reported by Xie et al.; (b) pyrolytic graphite from three literatures (Reproduced from Ref. [12] with permission from the Royal Society of Chemistry.)

By fitting the  $\Theta$ - $T$  curves, the Debye temperature can be extracted. Experimentally,  $\theta$  is always measured by low-temperature heat capacity measurement or neutron scattering studies. The thermal reffusivity theory provides an efficient alternative for estimating  $\theta$  of different materials.

In Xie's work,  $\theta$  of GF was determined to be  $1813 \pm 48$  K. This value was close to the average  $\theta$  value of three acoustic phonon mode in graphene, which is reasonable considering the existence of the impurities atoms in GF. For comparison, the  $\theta$  value of pyrolytic graphite was determined to be 1133–381 K, which were consistent with the reported value of graphene (1120 K) [13].  $\theta$  is the highest temperature of a crystal which can be achieved by single normal vibration. It has been proven to be a useful proxy for crystal rigidity, which is related to the strength of inner structural connectivity [14]. For example,  $\theta$  of nanoscale materials is generally smaller than that of the bulk counterpart. Part of the reason is phonon softening. In nanoscale materials, due to the size effect, the ratio of free/interfacial surface area to volume is much higher than that of bulk counterpart. Thus, the effect of free surfaces and grain boundaries is much more significant than that in bulk materials. As a result, the structure of nanoscale materials have 'looser' connectivity than that of the bulk counterpart. As a result,  $\theta$  is also reduced. In Cheng et al.'s work, the Debye temperature of silver nanowire determined from  $\rho_e$  profile (151 K) is much lower than that of the bulk silver (235 K) [10].

Since the defect scattering effect on thermal transport can be quantified from the  $\Theta_0$  value, subsequently, by taking out the defect scattering effect from the overall scattering, researchers were able to obtain the ideal thermal diffusivity ( $\alpha_{\text{ideal}}$ ) and conductivity ( $\kappa_{\text{ideal}}$ ) which are solely limited by phonon-phonon scattering. In Xie et al.'s work,  $\kappa_{\text{ideal}}$  of graphene in GF was reported for the first time [12].  $\kappa_{\text{ideal}}$  was obtained by  $\kappa_{\text{ideal}} = \rho c_p / (\Theta - \Theta_0)$ , in which  $\rho c_p$  is the volumetric specific heat of graphite. Before their work, researchers have been trying to characterize  $\kappa_{\text{ideal}}$  of graphene. For example, Chen et al. [15] measured the isotopically pure  $^{12}\text{C}$  graphene and reported the effect of different isotope compositions. The substrate scattering effect, size effect, impurities atoms effect on  $\kappa$  were also extensively studied. Nevertheless, the effect of different structural defects in the real materials could not be completely avoided. The thermal reffusivity theory, on the other hand, provides a simple and efficient way to subtract the defects scattering effect and evaluate  $\kappa_{\text{ideal}}$  of graphene in different graphene-based materials. This theory can also be extended to other materials whose thermal transport is dominated by phonons. However, it should be noted that this method for obtaining  $\kappa_{\text{ideal}}$  might not be always successful at very low temperatures. The phonon scattering cannot be always treated with the simple theoretical model.  $\tau_u$  and  $\tau_{\text{defects}}$  are different functions of phonon wave vectors. Thus, the Mathiessen's rule could become less accurate for summarizing the contribution of different phonon scattering mechanisms. Under this circumstance, the error of the estimated  $\kappa_{\text{ideal}}$  at low temperatures could be very large.

From the above analysis, thermal reffusivity of phonons

can be used to effectively evaluate the defect levels for nonmetallic materials, which has a much broader scope of application than electrical resistivity theory. For materials whose thermal transport is dominated by phonons, the Debye temperature of the materials, the effect of defects on the thermal conductivity, and the ideal thermal diffusivity/conductivity which is solely limited by the Umklapp phonon scattering can be extracted from the  $\Theta$ - $T$  curve and the value of  $\Theta_0$ .

## 5 Residual resistivity and structure domain size: crystalline materials

As temperature goes down, the lattice vibration weakens and the phonon population decreases. Thus,  $\tau_{\text{phonon}}$  increases and becomes ineffective in limiting  $\kappa$ . The effect of defect scattering dominates. At 0 K limit,  $\Theta_0$  reflects the defect scattering intensity from grain boundary, chemical impurities, lattice imperfections, rough edges, and amorphous structures, etc.. From Eq. (8), we can express  $\Theta_0$  in terms of the structural scattering mean free path  $l_0$  as  $\Theta_0 = 3/(v l_0)$ .  $l_0$  represents the mean free path limited by defect scattering.  $l_0$  is called structure thermal domain (STD) size as it reflects an effective size accounting for all the effects of grains on phonon-scattering. The STD size is comparable to the real crystallite size. However, it is not expected to precisely equal the crystalline size measured from XRD. XRD spectroscopy has been used for providing significant and detailed information about the crystallite size and structural order of materials in a specified direction. It generally evaluates the crystallite size by measuring the full width at half maximum (FWHM) of peaks. From each XRD peak, the average crystallite thickness along a specific lattice plane is obtained, while the thermal reffusivity model characterizes the STD size by considering the phonon scattering from all the lattice directions. Besides the direction along which the thermal reffusivity is measured, the diffusive scattering from the other two directions also contributes to limiting the STD size. Thus, the STD size is actually an effective domain size combining the effect from the three-dimensional crystallite.

In Cheng et al.'s work, the STD size of individual polycrystalline silver nanowire was determined to be 38.5 nm, which was larger than the value obtained from XRD result (21 nm in the (311) direction). The reason was that the STD size also included the phonon-mediated electron energy transfer across the grain boundaries, which resulted in a higher value than the crystallite size [10]. Xie et al. [12] evaluated the STD size of 3D graphene foam material synthesized by chemical vapor deposition. The value was reported to be 166 nm. For comparison, the crystallite size determined from XRD result was 201.8 nm corresponding to the (002) plane. These results demonstrated that the thermal reffusivity theory offers an alternative and

effective way to investigate the effective domain size of the samples. However, its value could be a little smaller or larger than the real crystallite size along one specific heat transport direction.

There are several points which should be noted when using  $\Theta$  for STD size evaluation. First, for 1-D heat conduction, we have  $\Theta_0 = (\nu l_0)^{-1}$ . In addition, to calculate the phonon velocity  $\nu$ , the contribution from all the phonon branches to the thermal transport should be taken into consideration. Liu et al. [16] characterized the STD size of two ultra-high molecular weight polyethylene (UHMWPE) fibers. The experimental result of thermal reffusivity of two PE fibers is shown in Fig. 4. The lines are polynomial fitting. The resulting  $\Theta_0$  values are also denoted in the figure. In their work, the heat conduction was regarded as 1-D due to the 1-D molecular structure. Thus, the STD size was calculated by  $l_0 = (\Theta_0 \nu)^{-1}$ . In addition,  $\nu$  was calculated by considering all the phonon branches as [17]

$$\frac{4}{\langle \nu \rangle^2} = \frac{1}{\langle \nu_{LA} \rangle^2} + \frac{1}{\langle \nu_{TA1} \rangle^2} + \frac{1}{\langle \nu_{TA2} \rangle^2} + \frac{1}{\langle \nu_{Tor} \rangle^2}. \quad (10)$$

In the  $c$ -axis,  $\nu_{LA}$ ,  $\nu_{TA1}$ ,  $\nu_{TA2}$  and  $\nu_{Tor}$  indicate the phonon velocity of longitudinal, transverse and torsional acoustic phonon branch [18]. The average  $\nu$  was calculated to be 3470 m/s. The resulting STD size were 7.3 and 8.7 nm for the two PE fibers. These values were much smaller than the crystallite size in the (002) direction determined

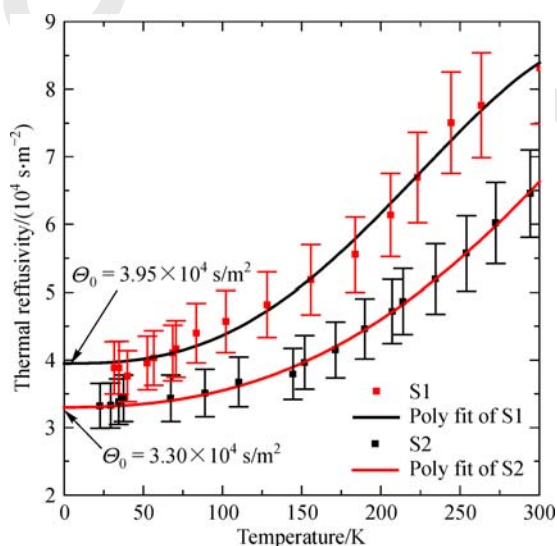


**Fig. 4** Thermal reffusivity of crystalline ultrahigh molecular weight polyethylene (UHMWPE) fibers (The residual thermal reffusivity was determined to be  $3.95 \times 10^4$  and  $3.30 \times 10^4$  s/m<sup>2</sup> for the two samples denoted as S1 and S2 respectively [16]. Adapted with permission from Liu J et al., *Acs Applied Materials & Interfaces*, 2015, 7(49): 27279–27288. Copyright (2015) American Chemical Society.)

from XRD results (19.7 nm). This revealed that the grain boundary scattering was very strong in PE fibers, which caused the phonons lost almost all the original information after passing the grain boundaries [16].

The thermal reffusivity model becomes advantageous in measuring very large crystallite size or very small volume samples. Many factors contribute to the observed XRD peak profiles including instrumental peak profile, crystallite size, microstrain, temperature factors, and so on. When the test material has very large crystallites, the broadening of crystallite size could become comparable or even much smaller than the instrumental peak width. Under this circumstance, the crystallite size cannot be accurately determined from XRD peaks. By contrast, the thermal reffusivity model can be used to effectively evaluate large crystallite size. For example, high quality graphene paper material (GP) was synthesized and extensively studied in recent years. Due to the very high in-plane order and ultra-low density of impurities and defects, the in-plane crystal size of GP is very large. Figure 5(a) shows the XRD result of GP material. Only one peak corresponding to the (002) plane was observed, which was very narrow and sharp. From this peak, the crystallite size along the thickness direction of GP was estimated to be larger than 300 nm. The peak width was comparable to the instrumental broadening, from which a reliable crystallite size along thickness direction cannot be extracted. The peak corresponding to (100) plane was not observable due to the extremely small scattering cross-section in the thickness direction. Thus, the in-plane crystallite size could not be extracted from XRD result either. Xie et al. utilized the thermal reffusivity model in the study of GP. The experimental result of  $\Theta$ - $T$  of GP is presented in Fig. 5(b). The STD size of GP along in-plane direction was effectively determined to be 1.68  $\mu$ m [19]. Besides the above situation, when sample volume or thickness is extremely small, like that for some nanofibers or 2D materials, XRD signals could be too weak for extracting the crystallite size. While with the last and sophisticated thermal characterization techniques nowadays,  $\Theta$  is easily measurable. Therefore, the thermal reffusivity theory plays complementary roles for XRD in characterizing the structural domain size of crystalline materials.

Furthermore, the STD size can be used for characterizing the structural evolution of crystalline materials. Liu et al. measured the STD size of carbon fibers before and after current-induced thermal annealing using the thermal reffusivity model. The results are summarized in Table 1. For two carbon fiber samples, the STD size after thermal annealing was reported to be 27.8%–72.2% larger than the original STD size [20]. The electrical resistance, thermal conductivity/diffusivity at RT, the residual thermal reffusivity are also presented in the table to show the annealing effect on improving the structure of carbon fibers. These results indicated that the current-induced thermal annealing successfully reduced the density of impurities and

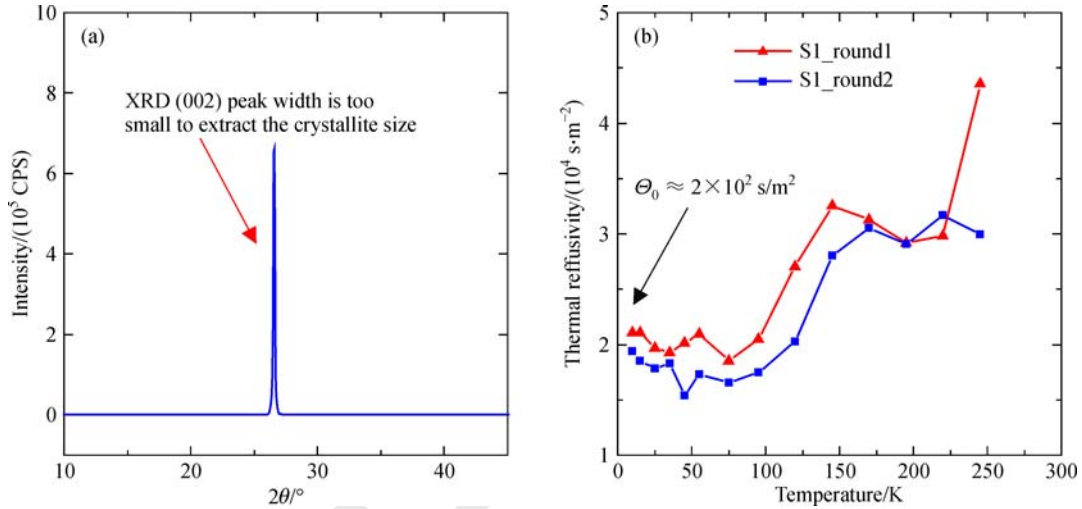


**Fig. 5** The XRD and low-temperature thermal reffusivity of high-quality GP for extracting crystallite size

(a) XRD result of the high-quality GP with large crystallite size (The crystallite size along thickness direction cannot be accurately evaluated since the peak width is comparable to the instrumental broadening); (b) thermal reffusivity of the high-quality GP against temperature (The in-plane STD size can be evaluated from the residual thermal reffusivity value. (Adapted from Ref. [19] with permission from the Royal Society of Chemistry.))

**Table 1** The annealing effect on the structural domain size of carbon fibers. Summarization and comparison of electrical resistance, thermal conductivity/diffusivity at RT, residual thermal diffusivity and STD size [20]. (Reprinted from Carbon, 121, Liu et al., Thermal conductivity and annealing effect on structure of lignin-based microscale carbon fibers, 35–47., Copyright (2017), with permission from Elsevier.)

Index		$R/\Omega$	$\kappa/(W \cdot (m \cdot K)^{-1})$	$\alpha/(m^2 \cdot s^{-1})$	$\Theta_0/(s \cdot m^{-1})$	$l_0/nm$
S6	Pre-annealed	136	2.0	$1.36 \times 10^{-6}$	$7.13 \times 10^5$	0.9
	Post-annealed	67.7	2.9	$1.88 \times 10^{-6}$	$4.11 \times 10^5$	1.55
S7	Pre-annealed	149.4	1.65	$1.07 \times 10^{-6}$	$8.10 \times 10^5$	0.79
	Post-annealed	104.4	2.0	$1.34 \times 10^{-6}$	$6.31 \times 10^5$	1.01

defects in the carbon fiber materials. As a result, the phonon mean free path induced by static defects and impurities was significantly increased. The structural improvement can be clearly seen from the comparison of STD size of pre-annealed and post-annealed samples. Xie et al. [19] compared the STD size of graphene oxide paper (GOP), partly-reduced graphene paper (PRGP), and GP. The STD size were reported to be 5.9 Å for GOP, 4.6 Å for PRGP, and 1.6 μm for high quality GP. For comparison, XRD spectroscopy also gave the crystallite size of these three materials, which were 71 Å for GOP, 48 Å for PRGP, and > 300 nm for GP. The value of the STD size was much lower than the size obtained from XRD, but the conclusion on the structural comparison for the three materials were consistent. From these result, the average sp<sup>2</sup> domain size experienced an increasing-then-decreasing pattern during reduction process from graphene oxide to high purity graphene. This observation was also reported for chemical reduction process (from graphene oxide to graphene) which was studied by Raman spectroscopy [21,22].

## 6 Residual resistivity and structure domain size: amorphous materials

Amorphous structure is a wide-spread existence with numerous applications. For example, polymers generally have amorphous structures. Amorphous materials-based thin films play a growing role in emerging semiconductor devices, optical coating, transistors, and thin film solar cell, etc. Examples include deposited thin films on a substrate, such as few-nm thin SiO<sub>2</sub> film in the metal-oxide semiconductor field-effect transistor. An in-depth understanding of the relation between amorphous structures and their thermal behaviors is of significant importance for their application and thermal design. Compared with crystalline materials, amorphous solids lack long-range order. However, they still have short-range order at atomic scale due to the nature of chemical bonding. Thus, amorphous solids also have corresponding domain structures which reflect the level of structural order. The amorphous domains are constrained by grain boundaries

and might contain local crystal structures (e.g.  $\alpha$  helix and  $\beta$  sheets in proteins), which makes the domains observable by few analytic techniques, including nuclear magnetic resonance (NMR) spectroscopy, XRD, Raman spectroscopy, etc. [23–25].

Nevertheless, structural domain size characterization of amorphous solid is challenging for the existing techniques. The domain size is normally characterized by XRD in crystalline solids. In amorphous materials, the crystal size is sufficiently small. As a result, the crystalline diffraction peaks may broaden and merge into each other, which forms a single broad diffraction peak (halo) in XRD result. This makes XRD not applicable for characterizing domain size of amorphous materials [26]. Besides XRD, Raman spectroscopy has been used for evaluating the domain sizes not only in crystallite materials but also in amorphous solids [27,28]. By measuring the line width of Raman peaks, a domain size can be extracted, which is induced by the limited phonon lifetime reduction by grain boundaries [29]. However, when measuring amorphous materials, researchers always found themselves in the dilemma of obtaining weak Raman signal or suffering from fluorescent interference. NMR spectroscopy is a technique that exploits the magnetic properties of certain atomic nuclei. It is difficult to use NMR to analyze large molecules, while typical biomolecules like proteins are large molecules [30].

Unlike crystallite materials, amorphous materials lack long-range translational symmetry and periodicity. From a practical perspective, researchers attempted to reinterpret phonon model for amorphous solids in the past five decades [31,32]. An explanation is that amorphous solids are highly defective crystals, in which phonons are considered localized. Therefore, like that in crystalline materials, the domain size of amorphous materials can also

be characterized by phonon mean free path at the 0 K limit.

The thermal reffusivity theory provides a convenient and effective way to study the domain size in amorphous structures. Its application in amorphous materials was first carried out by Xu et al. [33] on  $\lambda$ -DNA nanofibers. Figure 6(a) shows the SEM image of the DNA fiber sample. The thermal reffusivity of the DNA fiber samples is shown in Fig. 6(b).  $\Theta_0$  was measured to be  $0.4 \times 10^6$  s/m<sup>2</sup>. With an average phonon velocity of 3734 m/s in DNA, the STD size in the  $\lambda$ -DNA nanofiber was estimated as 0.67 nm [8]. This size is the average length that a phonon will be scattered by structural domains to lose its original energy information. It is very interesting to note that in the DNA nanofiber, the measured STD size was twice the reported base pair length of DNA (0.34 nm) [8], as illustrated in the inset of Fig. 6(b). Thus, the STD size offered an effective estimation for the domain size in DNA fibers.

Herein, using the thermal reffusivity theory, the structural domain size of human hair with different colors (black and white) is characterized. The measured STD size is compared with the crystallite size obtained from XRD result. This study provides an excellent example for the application of thermal reffusivity theory in studying amorphous materials.

The thermal reffusivity ( $\Theta$ ) versus temperature of the two hair samples are measured using the transient electrothermal (TET) technique. TET technique is a fast and reliable technique for measuring the thermal diffusivity of solid materials, including conductive and nonconductive materials [34,35]. White and black human hair samples from a 27-year-old Chinese female are collected from the same hair strand. The hair color of this female is black in nature, while part of the hair turned white due to natural aging. The hair strand is black near the end (~15 cm) and

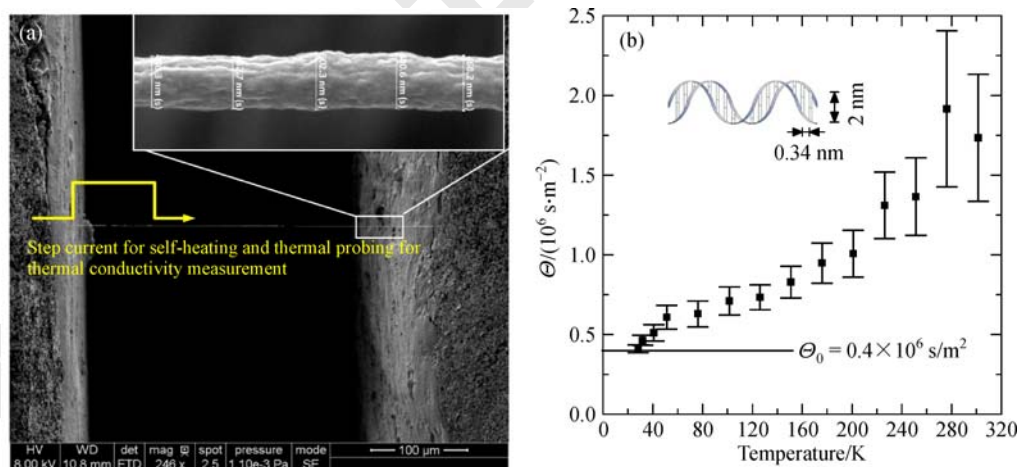


**Fig. 6** SEM image of  $\lambda$ -DNA nanofiber and its thermal reffusivity against temperature

(a) SEM image of the studied  $\lambda$ -DNA nanofiber suspended between two electrodes (Inset: A zoomed-in view of the  $\lambda$ -DNA nanofiber showing the diameter measurement); (b) thermal reffusivity of  $\lambda$ -DNA nanofiber against temperature (The residual thermal reffusivity is estimated to be  $0.4 \times 10^6$  s/m<sup>2</sup>. Inset of (b): characteristic scale of DNA [33]. (Reprinted from Polymer, 55, Xu et al., Promoted electron transport and sustained phonon transport by DNA down to 10 K, 6373-6380, Copyright (2014), with permission from Elsevier.))

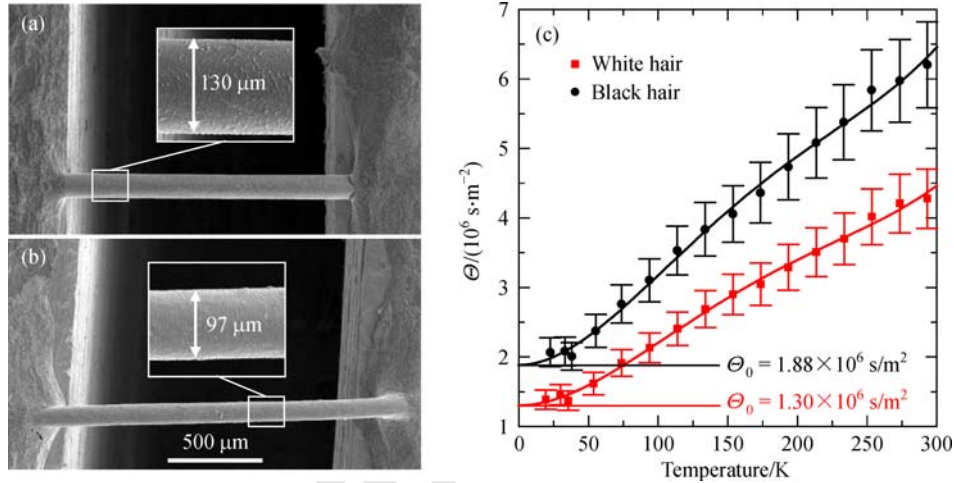


**Fig. 7** The SEM images and the thermal reffusivity profile of human hair

(a) The black hair sample; (b) the white hair sample (The samples are already coated with Iridium and suspended between electrodes for measurement. Insets of (a) and (b): zoomed-in view for diameter measurement); (c) thermal reffusivity as a function of temperature for both samples, with denoted residual thermal reffusivity (The lines are quadratic fitting curves, whose slope is fixed to zero at 0 K.)

white at the tip (~8 cm long). 1-cm cut is collected from the center of each color region. No chemical process is involved. For the TET measurement and SEM imaging, 20 nm Iridium coating is applied to both samples by sputter deposition (Quorum 150 T S) to make the samples electrical conductive. The SEM images and the diameter measurement of both coated samples are presented in Fig. 7(a) and (b).

The  $\Theta$ - $T$  result is shown in Fig. 7 (c). The contribution of radiation and Iridium coating to heat transport is evaluated to be less than 8% over the total thermal diffusivity and has been subtracted in the result. The physical model and process can be found in the Ref. [16].  $\Theta$  of white hair is lower than that of black hair by 42%–47% throughout the entire temperature range. This indicates a reduced level of phonon-phonon scattering in the white hair. The thermal diffusivity of the white hair is higher than that of the black hair. From a thermal protection perspective, the white hair loses part of the thermal protection function compared to that of the black hair. This is probably due to the loss of melanin (the protein associated with hair color) and the impaired inner structure. To further understand the reasons responsible for the different thermal properties, the thermal reffusivity theory is applied to study the phonon scattering and the STD size in the two hair samples in the following section.

The  $\Theta$ - $T$  of the black hair and white hair exhibit a common trend:  $\Theta$  decreases linearly with decreasing  $T$  as  $T > 50$  K; below 50 K,  $\Theta$  tends to be stable, leaving a residual value at 0 K. This behavior is different from the pattern of most of the crystallite materials and cannot be fitted using the thermal reffusivity model in Eq. (9). This linear  $\Theta$ - $T$  result is similar to that of carbon nanocoils material with polycrystalline-amorphous structure [36]. In their work, they attributed the linear behavior to the

combined scattering effect from both  $sp^2$  graphite grain and  $sp^3$  matrix. We speculate it to be a common behavior of materials with amorphous structures, but the coherent physical model and detailed explanation behind the linear  $\Theta$ - $T$  curves still require further future study.

Although the  $\Theta$ - $T$  result cannot be fitted using the thermal reffusivity model in Eq. (9),  $\Theta_0$  at 0 K limit still provides valid information on the defect levels and STD sizes. By using a quadratic fitting curve to smooth the data and fixing the slope at 0 K to be zero, the value of  $\Theta_0$  is determined to be  $1.30 \times 10^6$  s/m<sup>2</sup> and  $1.88 \times 10^6$  s/m<sup>2</sup> for the white hair and black hair, respectively. With an average phonon velocity in hair samples (1000 m/s), the domain size is estimated as 1.6 nm for the black hair and 2.31 nm for the white hair. Note that the average phonon velocity in hair is unknown so far, therefore the value used here is gauged from the determined values of other proteins [37]. Considering the phonon velocity in proteins is generally very low and within the same order of magnitude, the error from the phonon velocity is expected to be small. Larger STD size in the white hair sample reveals that the white hair contains less defect from the perspective of heat transport. Due to the loss of the melanin in the white hair, the inner structure of the white hair experienced a structural change which resulted in an increased domain size.

To validate our result on the STD size study, the domain size of the black hair sample is also characterized by XRD. The considerable embedded keratin crystals contribute to the broad peak as shown in Fig. 8. The crystallite size is determined to be 1.8 nm for the black hair. This value agrees well with the STD size (1.6 nm) derived from  $\Theta_0$ . This result firmly demonstrates that the thermal reffusivity theory does give a comparable evaluation on the domain size of human hair. It should be noted that for the human hair sample, XRD peaks are still not too broad to

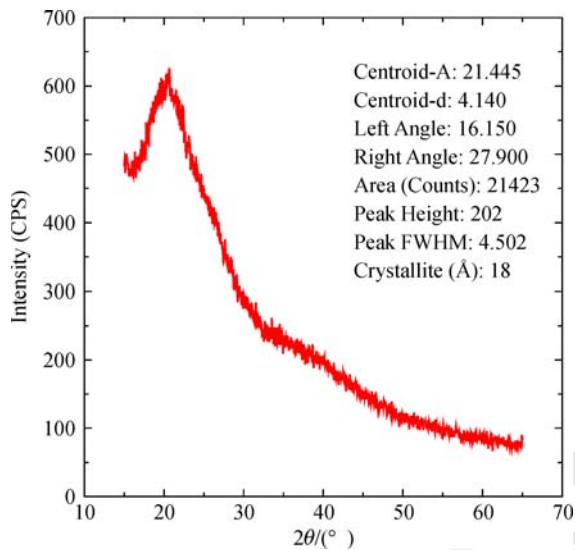


**Fig. 8** XRD pattern for human black hair (About 30 hair strands are aligned as a thin film for XRD characterization. The domain size, denoted as crystallite in the figure, is extracted from the width of the peak at 21.445°.)

overshadow the crystallite size information. However, this reaches a limit for the XRD study on amorphous materials. For other amorphous materials, such as silkworm silk, the XRD peaks are almost invisible. This makes the domain size characterization using XRD become impossible. In addition, the STD size of the black and white hair samples measured in this work is comparable to the value reported for other human hair specimens. A comparison between the thermal reffusivity theory and NMR was given by Kadir et al. [38]. For the studied virgin hair (Caucasian human), bleached hair, and perm-waved hair sample, the particle sizes in rigid phase were measured to be 4.5, 5.5 and 3.0 nm by  $^1\text{H}$  NMR analysis, respectively. For comparison, the STD values were measured to be 1.22, 1.97 and 1.75 nm, respectively. In spite of the difference in physical interpretation, the closeness of domain size values from both techniques postulated that grain size in human hair is about 1–5 nm.

## 7 Temperature-dependence of thermal reffusivity: uncovering the role of grain boundary phonon scattering

In addition to the function of extracting the Debye temperature, the way  $\Theta$  changes with  $T$  provides more information about the role of grain boundary scattering and strength of structural connection. For most of materials, the  $\Theta$ - $T$  curve presents a decreasing pattern as the temperature goes down and finally reaches a stable value  $\Theta_0$ . The thermal transport of this kind of materials is dominated by the Umklapp scattering at near RT and then by static defect

scattering at low temperatures. However, for some other materials, especially for some composite materials with loose structural connection, the  $\Theta$ - $T$  curve could present different behavior. The variation of  $\Theta$  against  $T$  offers a good indicator for analyzing the strength of boundary connection.

When the boundary connection is very weak in the test materials, the phonon scattering at boundaries would dominate the thermal transport in the whole temperature range. From Eq. (4) and (8), when  $\tau_{\text{defect}}^{-1}$  is much larger than  $\tau_{\text{phonon}}^{-1}$ , the effect of  $\tau_{\text{phonon}}^{-1}$  becomes negligible. As a result, the  $\Theta$  keeps almost constant at around the value of  $\Theta_0$ . Xie et al. [39] studied the thermal reffusivity of 3D graphene aerogel materials (GA) synthesized from chemical reduction using EDA as reduction agent. Figure 9(a) shows the  $\Theta$ - $T$  curve of GA [39].  $\Theta$  of group 2 presented only a very small variation against the temperature. GA materials were synthesized by graphene oxide flakes self-assembling during chemical reduction process. Thus, the inter-connection between graphene flakes are weak Van der Waals forces and  $\pi$ - $\pi$  stacking. Under this circumstance, the effect of grain boundary scattering was very significant and dominated the thermal transport in the whole temperature range from RT to 10 K. Since the defect scattering in GA was almost independent of temperature,  $\Theta$  of GA became almost invariant of temperature. This phenomenon was also reported for lignin-based microscale carbon fibers [20]. Thus, when the inter-connection strength inside the test materials is very weak, a constant  $\Theta$ - $T$  curve is expected.

In addition, for some composite materials,  $\Theta$  could even present a negative temperature coefficient. As temperature goes down,  $\Theta$  goes up. This phenomenon was observed for some composite materials with low thermal diffusivity. In Fig. 9(a),  $\Theta$  of the group 1 GA increases from  $2 \times 10^6$  s/m<sup>2</sup> to  $7 \times 10^6$  s/m<sup>2</sup>. The  $\Theta$ - $T$  curve of PRGP reported by Xie et al. is also presented in Fig. 9(b) [19]. From the curve, the  $\Theta$  presented a 100% increase from RT to 15 K. The negative temperature coefficient of  $\Theta$  indicated that the defect scattering intensity in these materials is not independent of temperature. The thermal transport in these materials are dominated by defect scattering. As temperature goes down, the interconnection among nanoparts is deteriorated. As a result, the phonon scattering intensity at the interfaces is increased, which causes the residual thermal reffusivity present a increasing pattern as temperature goes down. This phenomenon is always observed for materials with very low thermal diffusivity and complex nanostructures. The boundary scattering intensity is very high and can be affected by low temperatures.

## 8 Summary and future applications

Based on the electrons and phonons scattering mechanisms

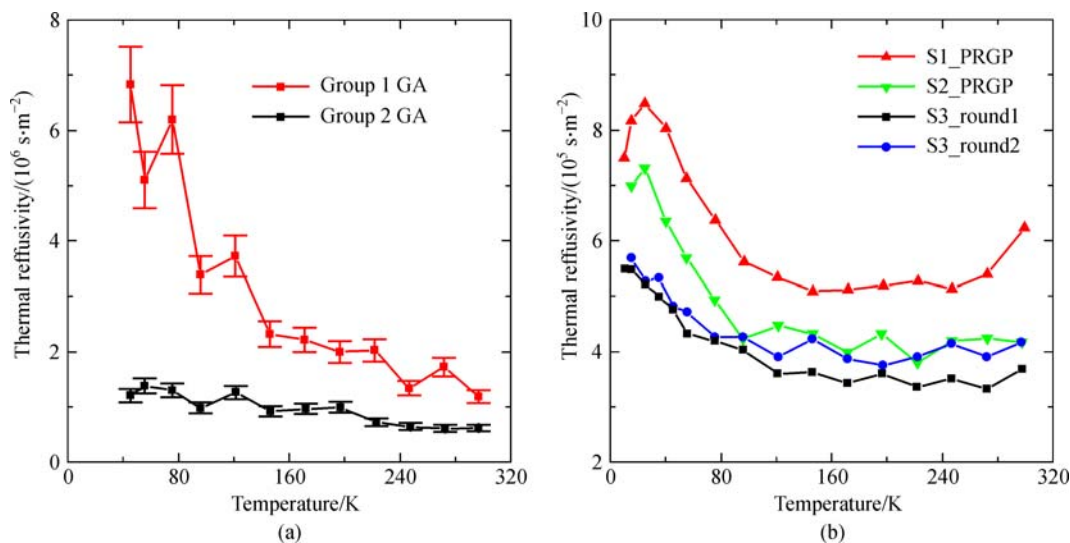


**Fig. 9** Thermal reffusivity against temperature profiles

(a) Graphene aerogel (GA) [39]; (b) partly reduced graphene paper (PRGP) (Reproduced from Ref. [19] with permission from the Royal Society of Chemistry.)

contributing to the thermal transport, a thermal reffusivity theory was developed in recent years and has been applied in the study of various materials including metals, semiconductors and organic materials. The definition and physical meaning of thermal reffusivity for metals and non-metals have been introduced in detail. The following applications of the thermal reffusivity model was then systematically reviewed. First, the proportion of the residual thermal reffusivity at 0 K limit over the thermal reffusivity at RT can be used as a measure of the defect levels in different materials. By fitting with the theoretical model, the Debye temperature and ideal thermal diffusivity can be evaluated. In addition, we highlighted that the structural thermal domain size of the materials can be obtained by using the residual thermal reffusivity value. For the materials with very large crystallite size or very small crystallite size (amorphous materials), the thermal reffusivity theory still provides an effective way for evaluating the structural domain size. This theory provides a good alternative and complement for other methods such as XRD. Ultimately, the profiles of the thermal reffusivity against temperature uncovers the role of boundary scattering and the strength of inner interconnection in the materials.

In this work, the comparison study between the white and black human hair from a same Asian woman from thermal protection perspective is reported for the first time. From this case study, the thermal reffusivity theory successfully evaluates the structural domain size of the human hair of black and white color. The value of STD size is comparable to the value obtained from the broad peak in XRD. With the help of  $\Theta_0$  and the STD size, the change of defects levels and domain size in human hair by losing

melanin is obtained. This proves the thermal reffusivity theory to be a useful tool for studying and comparing the structure of amorphous materials.

In the future, the application and study of thermal reffusivity theory are in demand in the following directions. The first direction is on 2D materials, such as graphene, black phosphorus,  $\text{MoS}_2$ , etc. The information on grain size is critical for the quality control, device design, and performance assessment of the 2D materials. However, due to the extremely small scattering cross-section in the thickness direction, XRD cannot generate enough signals for accurate in-plane crystallite size characterization. Using the thermal reffusivity theory, the structural thermal domain size can be obtained for these materials. This value will provide a good estimation of the real crystallite size by considering the phonon scattering effect from the three dimensions. In the second direction, the quantitative study on the structural domain size of amorphous materials becomes possible with the thermal reffusivity theory. This will shed light on a better understanding of the amorphous structures and the phonon scattering inside the structures. Finally, the residual thermal reffusivity at 0 K limit can be used for evaluating the defect levels of different kind of materials, including metals and nonmetals. The ideal thermal diffusivity of materials of perfect single crystal can be predicted using the thermal reffusivity theory. This provides an excellent experimental reference for calculation results.

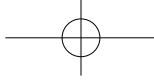
**Acknowledgements** Support of this work by National Science Foundation (CBET1235852, CMMI1264399), Department of Energy (DENE0000671, DE-EE0007686), and Iowa Energy Center (MG-16-025, OG-17-005) is gratefully acknowledged. Y. Xie is grateful to the China Scholarship Council for the great support.

## References

- Simon S H. *The Oxford Solid State Basics*. Oxford: Oxford University Press, 2013
- Jackson H E, Walker C T. Thermal conductivity, second sound, and phonon-phonon interactions in NaF. *Physical Review B: Condensed Matter and Materials Physics*, 1971, 3(4): 1428–1439
- Jackson H E, Walker C T, Mcnelly T F. Second sound in NaF. *Physical Review Letters*, 1970, 25(1): 26–28
- Kittel C, Allen K R. *Thermal physics*. *Physics Today*, 1970, 23(8): 61–63
- Kittel C, Holcomb D F. *Introduction to solid state physics*. *American Journal of Physics*, 1967, 35(6): 547–548
- Mayadas A F, Shatzkes M. Electrical-resistivity model for polycrystalline films—case of arbitrary reflection at external surfaces. 1970, 1(4): 1382–1389
- Chelikowsky J R, Louie S G. *Quantum Theory of Real Materials*. Berlin: Springer, 2012
- Xu Z L, Wang X W, Xie H Q. Promoted electron transport and sustained phonon transport by DNA down to 10 K. *Polymer*, 2014, 55(24): 6373–6380
- Clusius K, Losa C G. Low temperature research results XIV. The atomic and electronic heat of rhodium and irridium between 10°K and 273°K. *Zeitschrift Fur Naturforschung A*, 1955, 10(7): 545–551
- Cheng Z, Liu L, Xu S, Lu M, Wang X. Temperature dependence of electrical and thermal conduction in single silver nanowire. *Scientific Reports*, 2015, 5: 10718
- Kittel C, Masi J F. *Introduction to solid state physics*. *Physics Today*, 1957, 10(6): 43–44
- Xie Y S, Xu Z, Xu S, Cheng Z, Hashemi N. The defect level and ideal thermal conductivity of graphene uncovered by residual thermal reffusivity at the 0 K limit. *Nanoscale*, 2015, 7(22): 10101–10110
- Zhang J C, Huang X, Yue Y, Wang J, Wang X. Dynamic response of graphene to thermal impulse. *Physical Review B*, 2011, 84(23): 235116
- Denault K A, Brgoch J, Kloß S D, Gaultois M W, Siewenie J. Average and local structure, debye temperature, and structural rigidity in some oxide compounds related to phosphor hosts. *ACS Applied Materials & Interfaces*, 2015, 7(13): 7264–7272
- Chen S S, Wu Q, Mishra C, Kang J, Zhang H. Thermal conductivity of isotopically modified graphene. *Nature Materials*, 2012, 11(3): 203–207
- Liu J, Xu Z, Cheng Z, Xu S, Wang X. Thermal conductivity of ultrahigh molecular weight polyethylene crystal: defect effect uncovered by 0 K limit phonon diffusion. *ACS Applied Materials & Interfaces*, 2015, 7(49): 27279–27288
- Klemens P G, Pedraza D F. Thermal-conductivity of graphite in the basal-plane. *Carbon*, 1994, 32(4): 735–741
- Henry A, Chen G. High thermal conductivity of single polyethylene chains using molecular dynamics simulations. *Physical Review Letters*, 2008, 101(23): 235502
- Xie Y S, Yuan P, Wang T, Hashemi N, Wang X. Switch on the high thermal conductivity of graphene paper. *Nanoscale*, 2016, 8(40): 17581–17597
- Liu J, Qu W, Xie Y, Zhu B, Wang T. Thermal conductivity and annealing effect on structure of lignin-based microscale carbon fibers. *Carbon*, 2017, 121: 35–47
- Stankovich S, Dikin D A, Piner R D, Kohlhaas K A, Kleinhammes A. Synthesis of graphene-based nanosheets via chemical reduction of exfoliated graphite oxide. *Carbon*, 2007, 45(7): 1558–1565
- Hu H, Zhao Z, Wan W, Gogotsi Y, Qiu J. Ultralight and highly compressible graphene aerogels. *Advanced Materials*, 2013, 25(15): 2219–2223
- Kadir M, Wang X, Zhu B, Liu J, Harland D. The structure of the “Amorphous” matrix of keratins. *Journal of Structural Biology*, 2017, 198(2): 116–123
- Sarsfield B A, Futernik S, Hilden J L, Yin S, Young G. Powder X-ray diffraction detection of crystalline phases in amorphous pharmaceuticals. *Powder Diffraction*, 2006, 20(2): 178–178
- Gouadec G, Colombari P. Raman spectroscopy of nanomaterials: how spectra relate to disorder, particle size and mechanical properties. *Progress in Crystal Growth and Characterization of Materials*, 2007, 53(1): 1–56
- Svergun D I, Petoukhov M V, Koch M H J. Determination of domain structure of proteins from X-Ray solution scattering. *Biophysical Journal*, 2001, 80(6): 2946–2953
- Williams A C, Edwards H G M, Barry B W. Raman spectra of human keratotic biopolymers: skin, callus, hair and nail. *Journal of Raman Spectroscopy: JRS*, 1994, 25(1): 95–98
- Barhoumi A, Zhang D, Tam F, Halas N J. Surface-enhanced Raman spectroscopy of DNA. *Journal of the American Chemical Society*, 2008, 130(16): 5523–5529
- Xu S, Tang X, Yue Y, Wang X. Sub-micron imaging of sub-surface nanocrystalline structure in silicon. *Journal of Raman Spectroscopy*, 2013, 44(11): 1523–1528
- Matsuo H, Walters K J, Teruya K, Tanaka T, Gassner G T. Identification by NMR spectroscopy of residues at contact surfaces in large, slowly exchanging macromolecular complexes. *Journal of the American Chemical Society*, 1999, 121(42): 9903–9904
- Cahill D G, Pohl R O. Lattice vibrations and heat transport in crystals and glasses. *Annual Review of Physical Chemistry*, 1988, 39(1): 93–121
- Pohl R O, Liu X, Thompson E. Low-temperature thermal conductivity and acoustic attenuation in amorphous solids. *Reviews of Modern Physics*, 2002, 74(4): 991–1013
- Xu Z L. *Thermal transport in DNA*. Dissertation for the Doctoral Degree. Ames: Iowa State University, 2015
- Liu G Q, Lin H, Tang X, Bergler K, Wang X. Characterization of thermal transport in one-dimensional solid materials. *Jove-Journal of Visualized Experiments*, 2014(83): e51144
- Guo J Q, Wang X W, Wang T. Thermal characterization of microscale conductive and nonconductive wires using transient electrothermal technique. *Journal of Applied Physics*, 2007, 101(6): 063537–063537-7
- Deng C H, Sun Y, Pan L, Wang T, Xie Y. Thermal diffusivity of a single carbon nanocoil: uncovering the correlation with temperature and domain size. *ACS Nano*, 2016, 10(10): 9710–9719
- Achterhold K, Kepler C, Ostermann A, Van B U, Sturhahn W. Vibrational dynamics of myoglobin determined by the

- phonon-assisted Mössbauer effect. *Physical Review E*, 2002, 65(5): 051916
38. Kadir M, Wang X, Zhu B, Liu J, Harland D. The structure of the “amorphous” matrix of keratins. *Journal of Structural Biology*, 2017, 198(2): 116–123
39. Xie Y S, Xu S, Xu Z, Wu H, Deng C. Interface-mediated extremely low thermal conductivity of graphene aerogel. *Carbon*, 2016, 98: 381–390

Offprint  
Offprint



(contents continued from outside back cover)

- 121 **Siyuan CHENG, Xuguo SHI, Weigang MA, Xing ZHANG, Guanglai LIU, Mingxiang PAN, Weihua WANG**  
Experimental research on thermal transport properties of crystallized palladium-based alloys
- 127 **Dongchao XU, Quan WANG, Xuewang WU, Jie ZHU, Hongbo ZHAO, Bo XIAO, Xiaojia WANG, Xiaoliang WANG, Qing HAO**  
Largely reduced cross-plane thermal conductivity of nanoporous  $\text{In}_{0.1}\text{Ga}_{0.9}\text{N}$  thin films directly grown by metal organic chemical vapor deposition
- 137 **Pengfei JI, Yiming RONG, Yuwen ZHANG, Yong TANG**  
Impacts of cone-structured interface and aperiodicity on nanoscale thermal transport in Si/Gesuperlattices
- 143 **Yangsu XIE, Bowen ZHU, Jing LIU, Zaoli XU, Xinwei WANG**  
Thermal reffusivity: uncovering phonon behavior, structural defects, and domain size
- 158 **Xing FANG, C. Y. ZHAO, Hua BAO**  
Design and analysis of Salisbury screens and Jaumann absorbers for solar radiation absorption
- 169 **Kwang Hyun WON, Bong Jae LEE**  
Effect of light scattering on the performance of a direct absorption solar collector
- 178 **Yen-Hsiang CHEN, Li-Hung LIAO, Yu-Bin CHEN**  
Realization of energy-saving glass using photonic crystals
- 185 **Qing NI, Hassan ALSHEHRI, Yue YANG, Hong YE, Liping WANG**  
Plasmonic light trapping for enhanced light absorption in film-coupled ultrathin metamaterial thermophotovoltaic cells

**Special issue: Nanotechnology in energy (Guest editors: Changying ZHAO, Zhuomin ZHANG, Xing ZHANG)**

- 1 **Changying ZHAO, Zhuomin ZHANG, Xing ZHANG**  
Special issue: Nanotechnology in energy
- 5 **Eric TERVO, Elham BAGHERISERESHKI, Zhuomin ZHANG**  
Near-field radiative thermoelectric energy converters: a review
- 22 **Vishal TALARI, Prakhar BEHAR, Yi LU, Evan HARYADI, Dong LIU**  
Leidenfrost drops on micro/nanostructured surfaces
- 43 **Amun JARZEMBSKI, Cedric SHASKEY, Keunhan PARK**  
Review: Tip-based vibrational spectroscopy for nanoscale analysis of emerging energy materials
- 72 **Bin LIU, Lan DONG, Qing XI, Xiangfan XU, Jun ZHOU, Baowen LI**  
Thermal transport in organic/inorganic composites
- 87 **Guangzhao QIN, Ming HU**  
Thermal transport properties of monolayer phosphorene: a mini-review of theoretical studies
- 97 **Kai-Xuan CHEN, Min-Shan LI, Dong-Chuan MO, Shu-Shen LYU**  
Nanostructural thermoelectric materials and their performance
- 109 **Sevket U. YURUKER, Michael C. FISH, Zhi YANG, Nicholas BALDASARO, Philip BARLETTA, Avram BAR-COHEN, Bao YANG**  
System-level Pareto frontiers for on-chip thermoelectric coolers

*(contents continued on inside back cover)*

**Available online**

<http://www.springerlink.com>

能源前沿  
CN 11-6017/TK  
邮发代号: **80-972**

ISSN 2095-1701

